

CelloZIFPaper: Cellulose-ZIF Hybrid Paper for Heavy Metal Removal and Electrochemical Sensing

Hani Nasser Abdelhamid^{1,2*}, Dimitrios Georgouvelas¹, Ulrica Edlund³, Aji P Mathew^{1*}

¹Division of Materials and Environmental Chemistry, Stockholm University, Svante Arrhenius väg 16 C, Stockholm, SE-10691, Sweden

²Advanced Multifunctional Materials Laboratory, Department of Chemistry, Faculty of Science, Assiut University, Assiut, 71515, Egypt

³Department of Fibre and Polymer Technology, School of Engineering Sciences in Chemistry, Biotechnology, and Health, KTH Royal Institute of Technology, Teknikringen 56, Stockholm, SE-10044, Sweden

*Corresponding to Abdelhamid (hany.abdelhamid@aun.edu.eg); Mathew (aji.mathew@mmk.su.se)

Abstract

The processing of hierarchical porous zeolitic imidazolate frameworks (ZIF-8) into a cellulose paper using sheet former Rapid-Köthen (R.K.) is reported. The procedure is a promising route to overcome a significant bottleneck towards applying metal-organic frameworks (MOFs) in commercial products. ZIF-8 crystals were integrated into cellulose pulp (CP) or TEMPO (2,2,6,6-tetramethylpiperidine-1-oxyl radical)-oxidized cellulose nanofibrils (TOCNF) following an *in-situ* or *ex-situ* process; the materials were denoted as CelloZIFPaper_In Situ and CelloZIFPaper_Ex Situ. The materials were applied as adsorbents to remove heavy metals from water, with adsorption capacities of 66.2 - 354.0 mg/g. CelloZIFPaper can also be used as a stand-alone working electrode for the selective sensing of toxic heavy metals, for instance, lead ions (Pb²⁺), using electrochemical-based methods with a detection limit of 8 μM. The electrochemical measurements may advance 'Lab-on-CelloZIFPaper' technologies for label-free detection of Pb²⁺ ions.

Keywords: Metal-organic Frameworks; Cellulose; Processing; Paper Making; Water treatment; Metal Adsorption; Electrochemical-based sensing.

Introduction

Porous materials [1,2] such as Metal-organic frameworks (MOFs) [3–20] and zeolitic imidazolate frameworks (ZIFs) are hybrid porous materials consisting of metal ions connected with organic linkers [21–38]. Processing MOFs using template materials gives rise to a new class of mixed materials that combines the advantages of both components [21–26]. In recent years, hybridizing biopolymers such as cellulose with MOFs has resulted in the development of cellulose-MOF functional materials, which opens up vast new advantages in terms of high performance, good processability, and good sustainability [26]. Cellulose-MOFs have thereby several advanced applications, for instance, drug delivery [40,41], carbon dioxide (CO₂) adsorption [42], water remediation [43–45], thermal insulation, and fire retardancy [46]. Combining MOFs with cellulose offers significant processing flexibility, which is inherently limited for MOFs, using methods such as three-dimensional (3D) printing [40,47], freeze-drying [42], and sol-gel [48,49]. These methods can, among others, engineer cellulose-MOFs into scaffolds [40], elastic aerogels [46], foams [42], or coatings [50]. However, some of these methods require the use of a cellulose template for the *in-situ* growth of MOFs [51], complicated multi-step procedures [52], and the use of solvents or conditions harmful to the environment [26]. Thus, it is vital to develop facile cellulose-MOF processing methods that can be used in larger than lab-scale applications while using environmentally friendly conditions.

Water contamination with heavy metals is a critical issue for modern societies. The Agency for Toxic Substances and Disease Registry and the U.S. Environmental Protection Agency (EPA) recently published the 2019 Priority List of Hazardous Substances that stated the most toxic elements including several metal ions, e.g., arsenic (As), cadmium (Cd), mercury (Hg), lead (Pb), and selenium (Se) [53]. In this context, methodologies to remove as well as sense/detect these

ions are highly required to advance the water treatment. To that end, MOFs, among several other materials, offer the possibility for heavy metal removal via adsorption [26] as well as the detection of such contaminants using imaging-assisted sensing [54] and electrochemical and optical sensing [55].

This study reports the processing of ZIFs incorporated into cellulosic filter papers for the first time. It demonstrates the use of cellulose as a more environmentally friendly alternative to replacing inorganic or synthetic polymer substrates for ZIFs (sub-class of MOFs)-based paper fabrication [20]. We report the manufacturing of composite flat sheets consisting of ZIF-8 (or metal azolate framework-4, MAF-4) and different grades of cellulose, denoted as CelloZIFPaper, using Rapid Köthen flat sheet former. Both *in-situ* and *ex-situ* procedures are reported for the synthesis of CelloZIFPaper hybrid materials using TEMPO (2,2,6,6-tetramethylpiperidine-1-oxyl radical)-oxidized cellulose nanofibrils (TOCNF) as well as cellulose pulp (CP). The addition of CP facilitates the fabrication of flat sheets and allows the tuning of the structure of TOCNF-ZIF networks. The synthesis procedures are straightforward without needing a template or excessive harsh chemicals. They are mainly water-based and, in that respect, more environmentally friendly than other methods [52,56]. The CelloZIFPapers reported herein were evaluated for the adsorption and electrochemical sensing of heavy metal ions (Fe^{3+} , Cu^{2+} , Pb^{2+} , Co^{2+} , and Cd^{2+}). In addition, this study is the first example of 'lab-on-MOF' for the electrochemical sensing of toxic metal ions.

EXPERIMENTAL

Materials and Methods

Spruce cellulose pulp (CP) was obtained from Domsjö Fabriker AB (Sweden) in a never-dried form (17 wt.%) and was dispersed in water (0.3 wt.%) with extensive mixing (Ultra Turrax (IKA) at 15000 rpm for one h). $\text{FeCl}_3 \cdot 6\text{H}_2\text{O}$, $\text{CoCl}_2 \cdot 6\text{H}_2\text{O}$, $\text{Zn}(\text{NO}_3)_2 \cdot 6\text{H}_2\text{O}$, $\text{CuSO}_4 \cdot 5\text{H}_2\text{O}$, $\text{Pd}(\text{NO}_3)_2$,

$\text{Cd}(\text{NO}_3)_2 \cdot 4\text{H}_2\text{O}$, Na_2SO_4 , 2-methylimidazole (Hmim), nitric acid (68%), and triethylamine (TEA, anhydrous, $\geq 99\%$) were purchased from Sigma-Aldrich (Germany). TOCNF was prepared according to the previously reported method [57].

Synthesis of Cellulose/ZIFs and processing into CelloZIFPaper

The *in-situ* synthesis procedure involved the addition of the chemical reagents directly in the CP and TOCNF dispersions, separately. More specifically, $\text{Zn}(\text{NO}_3)_2$ (6 g) was added to the CP dispersion (0.3 wt.%) with stirring for 30 min before the addition of TEA (20 mL, 99.5%). The dispersions were stirred for one hour until a white precipitate was observed. Then, a solution of Hmim (60 mL, 0.84 M) was added, and the mixture was stirred for one hour. The same procedure was followed for the TOCNF dispersion (0.3 wt.%). Finally, the dispersions of CP/ZIF-8 and TOCNF/ZIF-8 were mixed in ratios of 1:0.5, 1:1, 1:2, and 1:4 using a total volume of 500 mL.

The *ex-situ* procedure involved the synthesis of ZIF-8 using the TEA-assisted method [58]. ZIF-8 was added in different amounts, 1.5 g, 3 g, 6 g, and 12 g, to 1 L of CP/TOCNF dispersion (CP/TOCNF ratio of 1:30 (wt.:wt.)) yielding a weight ratio of 1:0.5, 1:1, 1:2, and 1:4 (cellulose: ZIF-8, wt.:wt.), respectively.

The cellulose/ZIFs papers were fabricated using a Rapid Köthen 5-Automatic sheet former (Paper Testing Instruments GMBH, Austria) with a diameter of 200 mm. The materials were denoted as CelloZIFPaper_In Situ and CelloZIFPaper_Ex Situ using in situ and ex situ synthesis procedures. All mixtures, both in-situ and ex-situ, were mixed with Ultra Turrax for 30 min before sheet preparation to make them homogeneous. The total volume of the aqueous dispersions was 9 L to achieve long dewatering times and secure the homogeneity of the sheets. The dispersions were vacuum filtered through poly(vinylidene fluoride) filters (PVDF, pore diameter 0.65 μm , Merck)

to minimize the material losses. The papers were dried at 93 °C for 10 min under the pressure of 1 bar.

Characterizations

X-ray diffraction (XRD) was carried out using a PANalytical X'PertPRO X-ray diffractometer (Cu $K_{\alpha 1}$ radiation) using step size, current, and tension voltage of 0.05°, 40 mA, and 45 kV, respectively. Fourier-transform infrared attenuated total reflection (FTIR-ATR) spectroscopy was performed using a Perkin Elmer Spectrum 2000 FT-IR spectrometer. The particle size and morphology of the formed liquid phases during the *in-situ* synthesis were characterized using transmission electron microscopy (TEM, JEM 2100, JEOL, Japan, accelerating voltage 200 kV). The surface morphology and the cross-sections of the prepared papers were imaged using a scanning electron microscope (SEM, JSM-7000F, JEOL, accelerating voltage 2 kV). The loading of ZIF-8 onto CP and TOCNF was evaluated using energy-dispersive X-ray spectroscopy (EDX) with the same instrument. Nitrogen (N_2) adsorption-desorption isotherms were measured at 77 K using a Micromeritics ASAP 2020 instrument (U.K.). They were used for the calculation of specific surface areas using the Brunauer–Emmett–Teller (BET)[59] and the Langmuir methods [60]. The t-plot method was used for the calculation of the external surface areas. The pore size distribution was evaluated via the non-local density functional theory (NLDFIT) method using $N_2@77$ on a carbon slit. Metal concentration was estimated using atomic absorption spectrophotometer (FAAS) (Buck scientific 210VGC). X-ray photoelectron (XPS) analysis for the CelloZIFPaper_In situ before and after metal adsorption was recorded using Thermo Fischer (K-alpha, Al K_{α} radiation, 1486.6 eV). FT-IR for the material before and after adsorption was recorded using the KBr pellet method (Nicolet spectrophotometer, model 6700). Thermogravimetric analysis (TGA) was performed under air using Perkin Elmer TGA 7 thermal analyzer apparatus

(Shimadzu, Japan) at a heating and airflow rate of 10 °C/min, and 30 mL/min, respectively. The electrochemical measurements were recorded using CorrTest[®] (CS350, Wuhan, China). Diffuse reflectance spectroscopy (DRS) measurements before and after metal ions adsorption were recorded using Evolution 220 spectrophotometers coupled with ISA-220 integrating sphere (Thermo Fisher Scientific, U.K.). The bandgap energies of ZIF-8, CP, and CelloZIFPaper before and after metal adsorption were calculated using Tauc's plot according to Equation 1 [61]:-

$$(\alpha h\nu)^2 = A(h\nu - E_g) \quad \text{Eq.1}$$

Where h , ν , α , A , n , and E_g were Planck constant, frequency, absorption coefficient, constant, $n=2$, and bandgap, respectively. The photon energy ($h\nu$, eV) was calculated using wavelength (nm) using the equation; $h\nu = 1240/\lambda$.

Metal adsorption

The CelloZIFPapers were investigated for adsorption of Fe^{3+} , Co^{2+} , Cu^{2+} , Pb^{2+} , and Cd^{2+} from aqueous solutions. A 100 mg specimen of each sheet was added to the metal solutions (1000 ppm) and incubated for 12 h. The adsorption process was followed at a solution temperature of 23 ± 2 °C. The remaining metal concentration of each solution was measured via metal analysis using flame atomic absorption spectroscopy (FAAS). The changes in pH for the Pb^{2+} solution was recorded using a pH meter (Accumet[®] pH meter Model 810, Fischer Scientific).

The CelloZIFPaper_In Situ was investigated for the adsorption of Co^{2+} , Cu^{2+} , and Pb^{2+} from aqueous solutions. A 100 mg specimen of CelloZIFPaper_in situ (1:4 wt. ZIF: TOCNF) was added to the metal solutions (20 mL, 1000 ppm) and incubated for 12 h. The desorption was performed via stirring with acetonitrile (100 mL) for 12 h. The adsorption was recorded as percentage referring to the original adsorbed value of each metal ion. The recyclability of CelloZIFPaper was assessed following the same procedure for three cycles.

The adsorption of different amounts of Pb^{2+} was determined via soaking specimens (7 mg) of CelloZIFPaper into Pb^{2+} solutions with the volumes of 5, 10, 20, 50, and 100 mL (1000 ppm), respectively. The materials were incubated for 12 h. The materials were digested into nitric acid (68%). The concentration of Pb^{2+} metal ions was measured with FAAS.

Electrochemical analysis

Electrochemical experiments; cyclic voltammetry (CV), linear sweep voltammetry (LSV), potentiodynamic polarization test, chronoamperometry, and electrochemical impedance spectroscopy (EIS) were performed using a three-electrode cell including CelloZIFPaper ($1 \times 2 \text{ cm}^2$) as working electrode, a platinum mesh as a counter electrode, and Ag/AgCl electrode as a reference electrode. The measurements were performed in a Na_2SO_4 solution (0.1 M). Solutions of each metal ion (0.1 M) were dropwise applied onto the CelloZIFPaper in volumes of 0.1, 0.2, 0.3, 0.4, 0.5, 1, 2, and 3 mL. CV voltammograms were recorded at a potential scan rate of 50 mV/s from +0.6 to +0.2 V vs. Ag/AgCl. The EIS spectra were recorded at a potential of 0.2 V vs. Ag/AgCl in the frequency ranges from 100 kHz to 0.01 Hz with an amplitude perturbation potential of 10 mV.

Results and Discussion

Characterization of Materials and CelloZIFPaper

The *ex-situ* and *in-situ* synthesis procedures are schematically represented in **Fig. 1**. The *ex-situ* synthesis procedure includes two steps: 1) TEA-assisted synthesis of ZIF-8 crystals and 2) synthesis of cellulose/ZIF-8 via different weight ratios. The *in-situ* synthesis procedure involves successive chemical reagents of $\text{Zn}(\text{NO}_3)_2$, TEA, and organic linker Hmim (**Fig. 1**). The dispersions were processed into sheets using a Rapid Köthen sheet former yielding sheets with

diameters of 200 mm (**Fig. 1**). The sheets were characterized using XRD (**Fig. S1**), TEM (**Fig. 2**), XPS (**Fig. 3**), SEM (**Fig. 4**), FT-IR (**Fig. S2**), N₂ adsorption-desorption isotherms (**Fig. S3-S4**), TGA (**Fig. S6**), CV (**Fig. S7**), LSV (**Fig. S7**), and EIS (**Fig. S8**). The phases formed during the synthesis were also characterized with XRD (**Fig. S9**), FT-IR (**Fig. S10**), and TEM (**Fig. 3**).

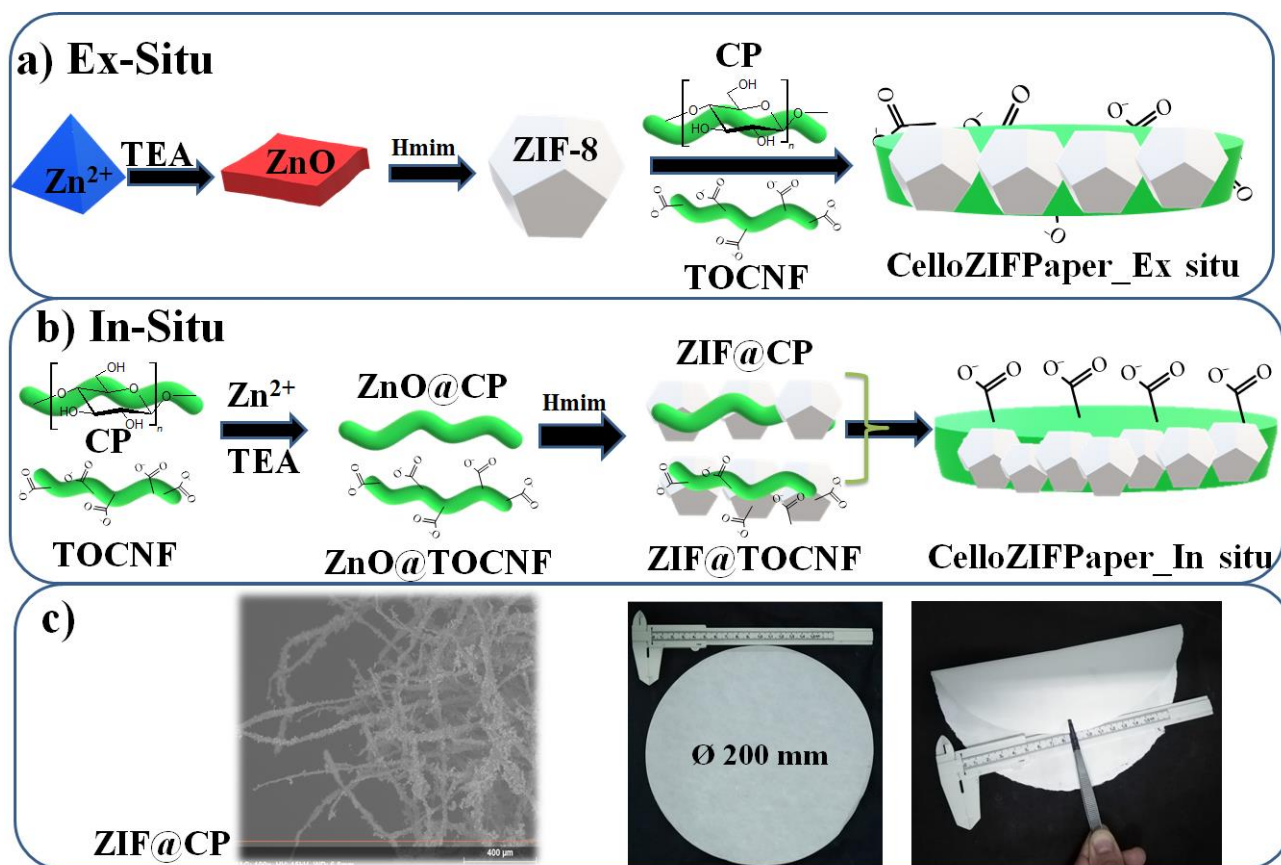


FIGURE 1 Schematic representation of the synthesis and processing of Cellulose/ZIF-8 into a paper sheet via a) *Ex-situ* and b) *In-situ* procedures, and c) shows SEM image of a cellulose pulp/ZIF-8 dispersion synthesized via the *in-situ* procedure, and camera image shows a membrane with a diameter size of 200 mm as an example with and without folding.

XRD patterns for the *in-situ* synthesis procedure in the presence of CP and TOCNF confirm the successful synthesis of a pure phase of ZIF-8 crystals (**Fig. S1a**). This observation indicates no negative impact of CP or TOCNF on the crystal growth of ZIF-8 materials. XRD pattern for the white precipitate formed during the *in-situ* procedure stated the presence of zinc oxide (ZnO) and

zinc hydroxide nitrate ($\text{Zn(OH)}_8(\text{NO}_3)_2 \cdot 2\text{H}_2\text{O}$, JCPDS card 24-1460) (Fig. S8)[62]. XRD patterns of CP or TOCNF show peaks at 15.3° , 16.9° , 22.7° , and 34.9° corresponding to Miller indices of (1 $\bar{1}$ 0), (110), (200), and (004), respectively [63]. After the crystal growth of ZIF-8, the prominent peak at 22.7° was preserved, indicating the presence of cellulose in the final products (**Fig. S9**). The transformation of ZnO into ZIF-8 crystal is fast and requires 30 min [58]. TEM images of the observed phases indicate the presence of ZnO crystals with a particle size of 500 nm (**Fig. 2a-b**).

The interactions between the functional groups of CP and TOCNF, respectively, were characterized using FT-IR (**Fig. S10**). The FT-IR spectrum of CP shows characteristic peaks at 3300 cm^{-1} , 2900 cm^{-1} , 1638 cm^{-1} , 1306 cm^{-1} , and 890 cm^{-1} corresponding to stretching vibration of O-H, C-H, bending H-O-H, C-O, and C-O-C vibration for β , 1,4-glycosidic linkage, respectively (**Fig. S10**). A new peak, assigned to Zn-O, at $422\text{-}425\text{ cm}^{-1}$ was observed after adding TEA to cellulose/ Zn^{2+} (**Fig. S10**). The crystal growth of ZIF-8 materials in the presence of CP or TOCNF can be confirmed from the Zn-N bond at 420 cm^{-1} (**Fig. S10**). The signal at 420 cm^{-1} is preserved after the processing into CelloZIFPaper, indicating the presence of ZIF-8 crystals in the final product. The successful synthesis of ZIF-8 can be confirmed from the XRD pattern of the paper that shows the characteristic diffraction pattern for ZIF-8 crystals (**Fig. S1**). The diffraction patterns of the paper proceeding using the *ex-situ* synthesis procedure show firm diffraction peaks for ZIF-8 compared to the paper prepared via the *in-situ* procedure (**Fig. S1**).

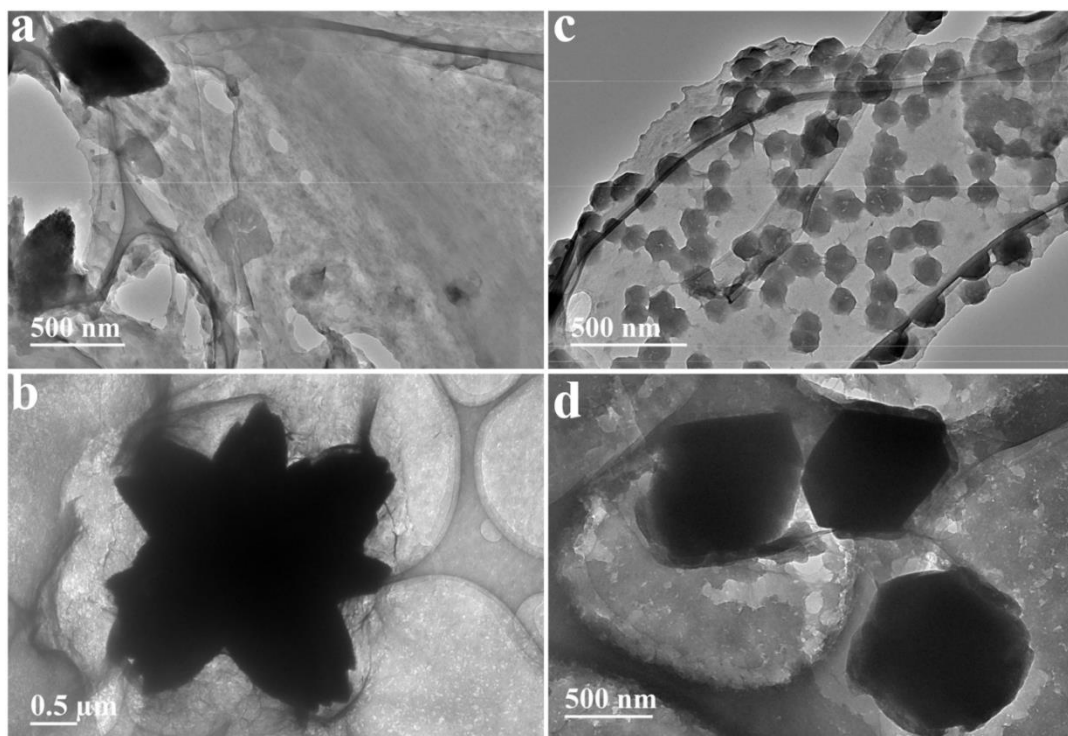


FIGURE 2 TEM images for a) ZnO/CP, b) ZnO/TOCNF, c) ZIF-8/CP, and d) ZIF-8/TOCNF.

The chemical bonds between cellulose (e.g., CP and TOCNF) and ZIF-8 inside CelloZIFPaper_In Situ and CelloZIFPaper_Ex Situ were characterized using XPS analysis (**Fig. 3**). The elemental survey for the materials verifies the presence of Zn, O, C, and N (**Fig. 3a**). The XPS analysis of O 2p for CelloZIFPaper_In Situ shows peaks at a binding energy of 533.1 eV, 532.2 eV, and 531.4 eV corresponding to C-O, C=O, and Zn-O, respectively (**Fig. 3b**). Spectrum analysis of O 2p of CelloZIFPaper_Ex Situ shows only two peaks at the binding energy of 532.9 eV and 532.1 eV corresponding to C-O C=O, respectively (**Fig. 3b**). The data analysis indicates a stronger interaction between TOCNF and ZIF-8 crystals using the *in-situ* synthesis procedure than the *ex-situ* procedure. This observation can be confirmed from the study of Zn 2p (**Fig. 3c**) as well. Both hybrid papers, i.e., CelloZIFPaper_In Situ and CelloZIFPaper_Ex Situ, show peaks at binding energies of 1045.3 eV and 1022.2 eV corresponding to Zn 2p_{1/2} and Zn 2p_{3/2}, respectively (**Fig. 3c**). However, an extra peak corresponding to Zn-O was observed at a binding energy of 1024.4

eV for CelloZIFPaper_In Situ (**Fig. 3c**). XPS analysis indicates a stronger interaction between TOCNF and ZIF-8 crystals inside CelloZIFPaper_In Situ than CelloZIFPaper_Ex Situ. This was further sustained by observing the leaching of white particles upon touching the papers synthesized via *ex-situ* synthesis procedure, probably, due to loosening binding to cellulose particles.

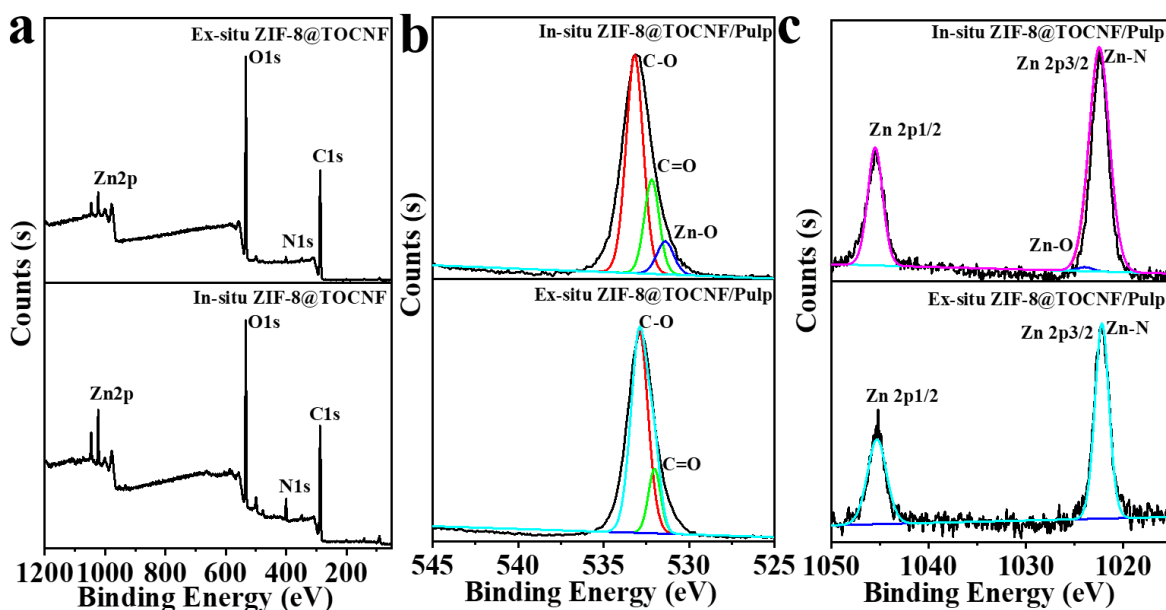


FIGURE 3 XPS spectra for ZIF-8/TOCNF membranes prepared via *in-situ* and *ex-situ* procedures, a) survey, b) O 2p, and c) Zn 2p.

The crystal morphology and particle size in dispersion and CelloZIFPaper were evaluated using TEM (**Fig. 2c-d**) and SEM imaging (**Fig. 4**). The *in-situ* growth of ZIF-8 in CP gives rise to smaller particles (average crystal particle size of 40 nm) than the ZIF-8 crystals grown in the presence of TOCNF (average crystal particle size 250 nm, **Fig. 2c-d**). ZIF crystals can be *in-situ* synthesized on the cellulose fibrils of CP (**Figure 1c**). SEM images of CelloZIFPaper_In Situ show homogenous crystal distribution within the membrane (**Fig. 4a-c**). Additionally, the amount of ZIF-8 crystals increases with the increase of the loading of CP/TOCNF and ZIF-8 (i.e., higher ratio values) from 1:0.5 (**Fig. 4d-f**) to 1:4 (**Fig. 4g-i**). TEM and SEM images show mesoporous structure

inside the ZIF-8 crystal, indicating that the synthesis procedure yields hierarchical porous ZIF-8. Material porosity was determined using nitrogen adsorption-desorption isotherms (**Fig. S2**). Specific surface areas (BET and Langmuir), external surface area, and pore volumes are summarized in **Table 1**. When the *ex-situ* synthesis procedure was applied, the surface area increased with ZIF-8 loading (**Table 1**). From the collected data, one can observe that both *in-situ* and *ex-situ* prepared papers with the lowest ratios (1:0.5) have the highest ZIF-8 loading (**Table 1**). The *in-situ* synthesis procedure yielded higher ZIF-8 loading (70 wt.%) compared to the *ex-situ* synthesis procedure (59 wt.%) at the low ratio of 1:0.5 (**Table 1**). CelloZIFPaper was fabricated with a diameter of 200 mm and can be folded without significant damage (**Figure 1c**).

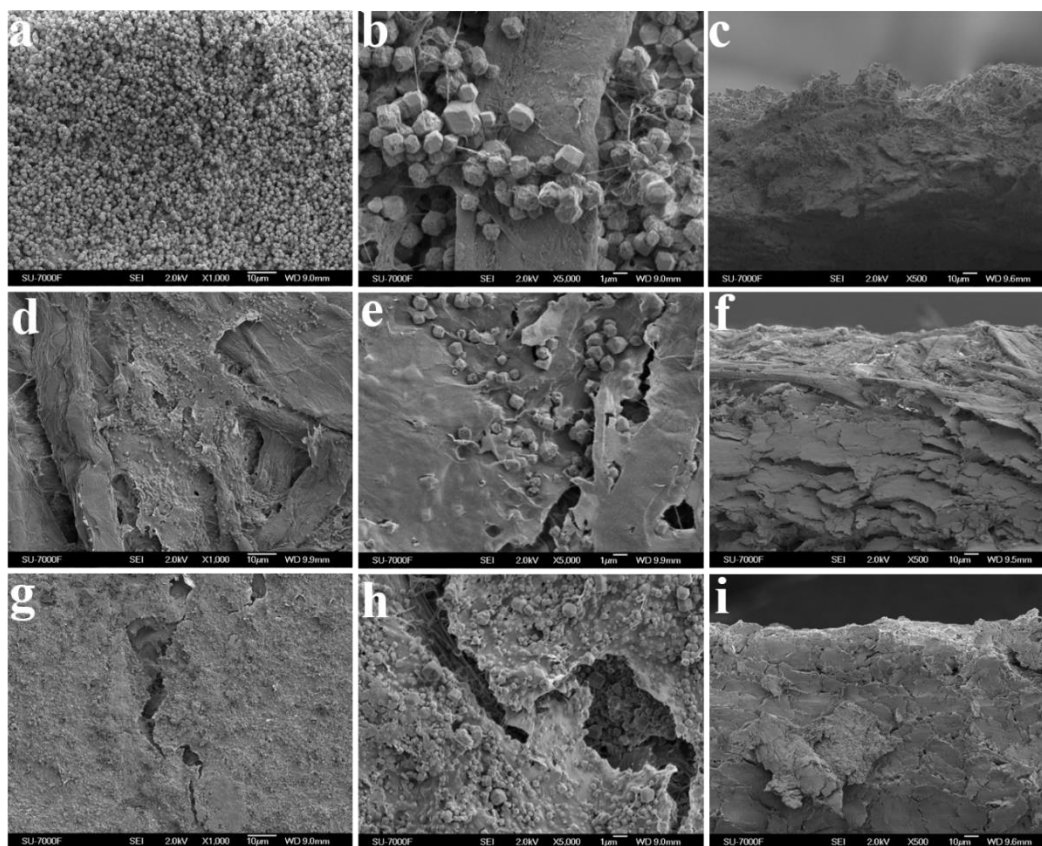


FIGURE 4 a, b, d, e, g, h) SEM images of CelloZIFPaper and their cross-sections c, f, i). CelloZIFPapers were prepared via a-c) *ex-situ* procedure and d-i) *in-situ* procedure using cellulose: ZIF ratio of d-f) 1:0.5 and g-i) 1:4.

Table 1 Summary of surface area, pore-volume, and ZIF-8 loading of the prepared CelloZIFPaper samples.

	Cellulose: ZIF	Zn (%) ^a	ZIF (%)	S _{BET}	S _{Lan}	S _{Ext}	V _{Total}	V _{Micro}	V _{Meso}
				m ² /g			cm ³ /g		
<i>ZIF-8</i>	0:100		100	980	1130	650	0.44	0.34	0.10
<i>Ex-situ</i>	1:0.5	16.9 ± 1.4	59	27	35	13	0.016	0.006	0.01
	1:1	11.6 ± 1.4	42	60	80	20	0.035	0.02	0.015
	1:2	12.5 ± 1.0	44	95	120	25	0.05	0.03	0.02
	1:4	12.4 ± 1.4	44	100	130	27	0.06	0.03	0.03
<i>In-situ</i>	ZIF-8@CP	4.8 ± 0.35	17	230	310	60	0.11	0.07	0.04
	ZIF-8@TOCNF	17.0 ± 1.4	59	230	300	60	0.14	0.07	0.07
	1:0.5	19.6 ± 1.4	70	6	8	9	0.01	0.001	0.009
	1:1	8.8 ± 0.7	31	6	6	8	0.04	0.001	0.039
	1:2	8.0 ± 0.7	28	9	12	11	0.026	0.001	0.025
	1:4	8.5 ± 1.0	30	10	11	14	0.025	0.001	0.024

Notes: a, based on EDX analysis for Zn; S_{BET}, specific surface area calculated using BET; S_{Lan}, Langmuir surface area; S_{Ext}, External surface area; V_{Total}, total pore volume; V_{Micro}, micropore volume; V_{Meso}, mesopore volume; Cellulose refers to the sum of CP and TOCNF.

Adsorption and Electrochemical-based Sensing of Heavy Metals

Adsorption of heavy metals

The CelloZIFPapers with the highest ZIF-8 content were evaluated for heavy metal adsorption capacity using aqueous solutions of Cd²⁺, Co²⁺, Cu²⁺, Fe³⁺, and Pb²⁺ (**Fig. 5**). The metal adsorption using ZIF-8 is usually fast [64,65]. The adsorption equilibrium for Co²⁺ ions can be achieved after 30 min (**Fig. 5a**). The fast adsorption can also be confirmed from the fast color change of the CelloZIFPaper from white to blue or purple after the soaking into Cu²⁺ or Co²⁺ ions solution, respectively, after 10 min. CelloZIFPaper_In Situ exhibited higher adsorption capacity than CelloZIFPaper_Ex Situ. The materials exhibited adsorption capacities of 143, 350, 354.0, 260.8, and 307.3 mg/g for Cd²⁺, Co²⁺, Cu²⁺, Fe³⁺, and Pb²⁺ ions, respectively (**Fig. 5b**). On the other hand, CelloZIFPaper_Ex Situ showed adsorption capacities of 196.8, 300, 166.5, 66.2, and 87.2 mg/g for Cd²⁺, Co²⁺, Cu²⁺, Fe³⁺, and Pb²⁺, respectively (**Fig. 5b**). There is no significant Zn leaching

during the adsorption (**Fig. 5a**). The adsorption of Pb^{2+} using CelloZIFPaper_In Situ increased with the initial metal ion concentration (**Fig. 5c**).

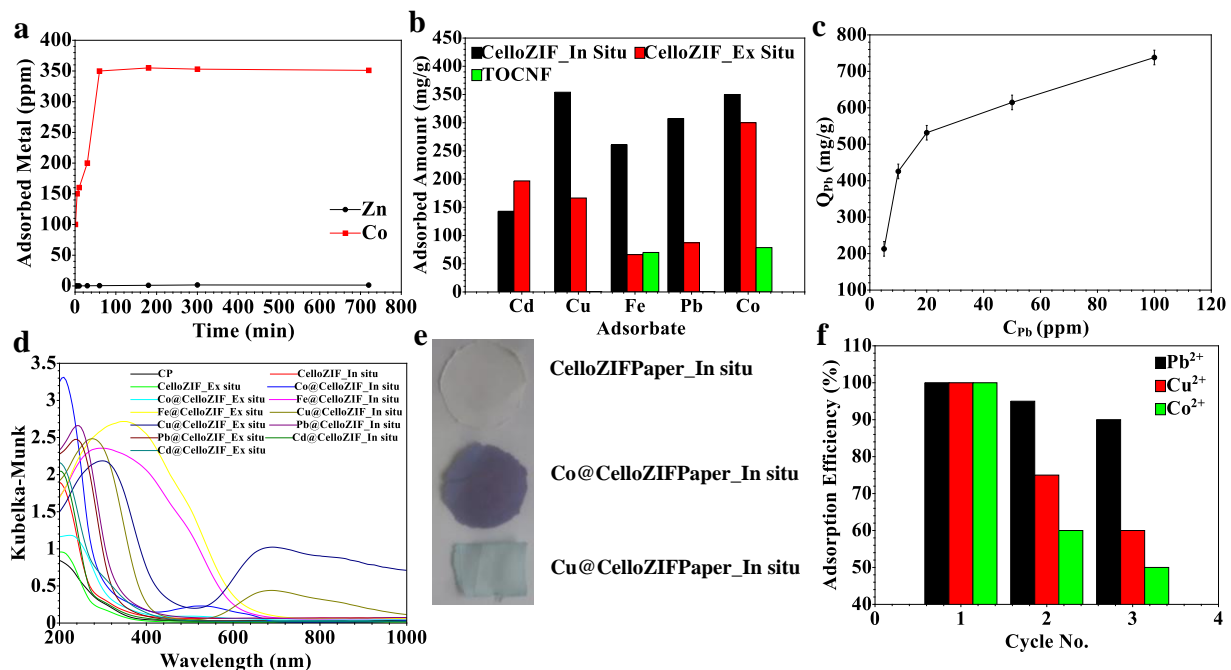


FIGURE 5 a) Kinetic adsorption and Zn leaching, b) Adsorption capacity of the CelloZIFPaper and TOCNF for metal ions. The adsorption of Fe^{3+} and Co^{2+} was reused from our previously published article using only TOCNF, Ref. [66], c) adsorption of Pb^{2+} as a function of initial concentration, d) DRS for CelloZIFPaper before and after metal ion adsorption, e) camera image of CelloZIFPaper_In situ before and after adsorption of Co^{2+} and Cu^{2+} , and f) recyclability for metal ions adsorption.

Several mechanisms for metal ion adsorption using ZIF8-based materials have been suggested [26,39,67]. The metal can be adsorbed using ZIF-8/TOCNF/CP via ion exchange (e.g., with a metal node of ZIF crystals) or coordination to the functional groups of cellulose (i.e., -O.H. or -COOH). In this work, pH changes (**Figure S11**), FT-IR (**Figure S12**), DRS (**Fig. 5d**), Tauc's plot (**Figure S13**) [61], XPS (**Fig. 6**), CV (**Fig. S14a-b**), and LSV (**Fig. S14c**) analyses were performed to elucidate the mechanism that controls these interactions. The Pb^{2+} solution is acidic, i.e., pH=4 (**Figure S11**). There is an increase in pH during the adsorption due to the removal of the metal ions (**Figure S11**). It was reported that ZIF-8 crystals provide a variety of active adsorption

sites, including O-H and N-H groups, low-coordinated Zn atoms, and free N⁻ groups belonging to Hmim [68]. Cellulose and TOCNF have functional groups such as O-H and COO⁻, adsorb metal ions [45]. FT-IR spectra for CelloZIFPaper before and after adsorption of metal ions are reported (**Figure S12**). Tetrahedrally coordinated atoms such as Co and Cu can replace Zn in the frameworks. FT-IR spectrum of CelloZIFPaper shows a peak at 421 cm⁻¹ corresponding to Zn-N (**Figure S12**). The FT-IR spectrum of Cu adsorbed CelloZIFPaper shows two peaks at 425 cm⁻¹ and 430 cm⁻¹ corresponding to Zn-N, and Cu-N, respectively (**Figure S12**). DRS spectra of the papers before and after metal adsorption indicate the change in the intensity of the UV-Vis absorption (**Fig. 5b**). This change can be attributed to the strong interaction between the adsorbed metal ions and the functional groups of the membranes that can be determined from Tauc's plot (**Figure S13**). The bandgap values of CelloZIFPaper before and after adsorption are tabulated in **Table S1**. The change in the bandgap of CelloZIFPaper reveals the presence of the adsorbed metal inside the crystal of ZIF-8. Thus, the white color of CelloZIFPaper turns purple and blue after the adsorption of Co²⁺ and Cu²⁺, respectively (**Figure 5e**). Other metal ions, such as Pb²⁺ or Cd²⁺, caused no dramatic change in the bandgap of CelloZIFPaper due to the low tendency for coordination inside ZIF-8 crystals (**Table S1**). The elemental survey for CelloZIFPaper_In Situ confirms the presence of C, N, Zn, and adsorbed metal species (**Fig. 6a**). XPS analysis of Pb@CelloZIFPaper_In Situ shows two peaks at binding energies of 143.9 eV and 138.9 eV corresponding to Pb 4f_{5/2} and Pb 4f_{7/2}, respectively (**Fig. 6b**). The Pb 4f_{7/2} peak reveals three peaks at binding energies of 137.8 eV and 140.4 eV, which are associated with Pb-O, and Pb-O-C, indicating the coordination to the carboxylic group of TOCNF (**Fig. 6b**). The analysis of the Cd adsorbed membrane shows two peaks at binding energies of 405.6 eV and 412.3 eV, corresponding to Cd 3d_{5/2} and Cd 3d_{3/2} (**Fig. 6c**). At the same time, the spectrum of the CelloZIFPaper used for

the adsorption of Fe^{3+} shows peaks at 711.0 eV, and 724.3 eV, corresponding to Fe 2p_{3/2} and Fe 2p_{1/2}, respectively (**Fig. 6d**). The Cu ion adsorbed paper analysis shows peaks at binding energies of 934.7 eV and 954.7 eV, corresponding to Cu 2p_{3/2} and Cu 2p_{1/2}, respectively, with two satellite peaks at 943.8 eV and 962.9 eV (**Fig. 6e**). The analysis confirms that the oxidation state of Cu is 2+ indicating no reduction of Cu^{2+} after adsorption (**Fig. 6e**). This observation suggests that the adsorption mechanism is different from the previously reported mechanism using only TOCNF, which causes the reduction of Cu^{2+} and formation of Cu_2O [69]. The ion-exchange mechanism for the adsorbed Cu^{2+} can be investigated via the analysis of N 1s (**Fig. 6f**). The XPS spectrum of N 1s of ZIF-8/TOCNF/CP paper shows two peaks at binding energies of 399.4 eV and 400.7 eV corresponding to $-\text{C}-\text{N}$ and $-\text{C}=\text{N}$ in Hmim, respectively [70]. After adsorption tests with the Cu^{2+} solution, the two peaks of N 1s for Hmim still exist, and an extra peak at 398.9 eV is observed, indicating the coordination between the nitrogen atom and Cu^{2+} (**Fig. 6f**). A previous study reported a new peak at a binding energy of 403.4 eV due to ion exchange and coordination between Cu^{2+} and ZIF-8 crystals [70]. This peak (at a binding energy of 403.4 eV) is not present in our case, indicating that the interactions are mainly electrostatic and coordination to N in Hmim. Both CelloZIFPaper_In situ and CelloZIFPaper_Ex situ after adsorption of Co^{2+} show a peak at a binding energy of 782.1 eV referring to $\text{Co}2\text{p}_{3/2}$ (**Fig. 6g-h**). The analysis of the adsorbed metal ions indicates that the adsorption takes place via coordination to the carboxylic groups of TOCNF or via electrostatic interaction without any observation of an ion-exchange mechanism. The adsorption of tetrahedral ions such as Cu^{2+} or Co^{2+} can be coordinated to the functional groups of ZIF-8, including O-H and N-H groups, low-coordinated Zn atoms, and free N^- groups belonging to Hmim [68]. Thus, these metals render the recyclability of the materials difficult using the desorption via acetonitrile compared to other metal ions such as Pb^{2+} (**Figure 5f**).

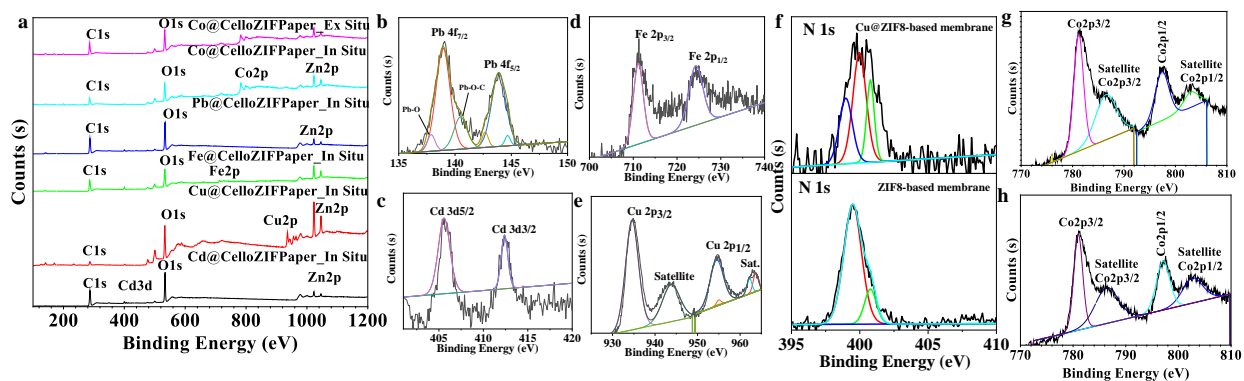


FIGURE 6 XPS analysis of CelloZIFPaper after the adsorption of metal ions, a) elemental survey, b) Pb 4f, c) Cd3d, d) Fe 2p, e) Cu 2p, f) N 1s, g-h) Co 2p for g) CelloZIFPaper_In situ and h) CelloZIFPaper_Ex situ.

MOFs-based materials are recognized as promising matrices for metal adsorption [71–74]. According to previous studies, ZIF-8 shows adequate metal ion adsorption (**Table 2**) [3,39,75]. However, this material lacks functional groups such as $-N-H$, $-O-H$, and $-COOH$ that facilitate the binding to metal ions; hence, adsorption can occur via either ion exchange [70] or intraparticle diffusion [76]. The adsorption of metal ions using ZIF-8 as an adsorbent can be further improved via conjugation with other nanomaterials, for instance, graphene oxide (GO) [77]. Removal of Cu^{2+} ions may occur via the coordination to the functional groups of GO without any observation of ion exchange with the Zn nodes of ZIF-8 crystals [77]. TOCNF and CP improved the metal ion adsorption compared to other materials (**Figure 5b**, **Table 2**). The preparation methods presented herein are fast and straightforward without needing a solvothermal procedure that requires a long reaction time (24 h) and high temperature (**Table 2**) [76]. A drawback of using ZIF sorbents in powder form is their tedious separation after the adsorption process. Thus, ZIF-8 was modified with magnetic nanoparticles to make their separation easier [78]. The use of our CelloZIFPaper allows the simple separation of the adsorbent without the need for any extra steps (**Table 2**). In a recent study, ZIF-8 nanoparticles were *in-situ* grown onto electrospun polyacrylonitrile (PAN)

nanofibers membrane (ZIF-8/PAN NF) via hot pressing [79]. ZIF-8 crystals were also produced on an alumina hollow fiber membrane via the *in-situ* solvothermal method and the layer-by-layer method (**Table 2**) [80]. This membrane fabrication method requires silanization of alumina with 2% of 3-(aminopropyl)triethoxysilane (APTES) solution using toluene which is toxic and harmful to the environment (**Table 2**) [80]. In contrast, the membrane preparation methods proposed in our study are entirely water-mediated, rendering them simpler and more environmentally friendly than the one mentioned earlier. Additionally, the CelloZIFPaper exhibited higher adsorption capacity toward heavy metal ions than several other adsorbents (**Table 2**).

Table 2 A comparison among different ZIF-based materials for heavy metal adsorption.

Form	Materials/ Membrane	Synthesis Conditions	ZIF (wt.%)	Metals	Capacity (mg/g)	Adsorption mechanism	Ref.
Powder	ZIF-8	RT, Stirred for 5 h	100	Cu ²⁺	800	Ion-exchange, coordination	[70]
		Solvothermal at 140 °C for 24 h		Cu ²⁺ Pb ²⁺	454.7 1119.80	Intra-particle diffusion	[76]
	ZIF-8@GO	1. Stirred at room temperature for 3 h 2. Vacuum drying oven for 12 h	92.2	Cu ²⁺	482.29	Coordination	[77]
	Fe ₃ O ₄ @ZIF-8	1. 200 °C for 8 h 2. RT, stirring for 2 h	45	Pb ²⁺ Cu ²⁺	719.42 301.33	Ion-exchange	[78]
		1. 90 °C for 1 h 2. RT, stirring for 30 min	90	Pb ²⁺ Cd ²⁺	666.7 833.3	Coordination	[3]
Membrane	TOCNF/Cellulose	Rapid Köthen	0	Cu ²⁺ Fe ³⁺	78.6 70.0	Electrostatic interactions	[66]
	ZIF-8/PAN NF	1. Electrospinning 2. Heated with a hot press at 80 °C	60	Cu ²⁺	225.62	Ion-exchange, coordination	[79]
	ZIF-8/alumina	1. Phase-inversion and sintering technique 2. Silanized in toluene for 2 h		Cu ²⁺	76.5	Ion-exchange	[80]
	CelloZIFPaper	<i>In-situ</i> procedure 1. Stirring, 1h 2. Rapid Köthen	70	Cd ²⁺ , Cu ²⁺ , Fe ³⁺ , Pb ²⁺ , Co ²⁺ ,	143.0, 354.0, 260.8, 307.3 350	Coordination, electrostatic interactions	This Work
		<i>Ex-situ</i> procedure 1. Stirring, 1h 2. Rapid Köthen	59	Cd ²⁺ , Cu ²⁺ , Fe ³⁺ , Pb ²⁺ , Co ²⁺ ,	196.8, 166.5, 66.2, 87.2 300		

Electrochemical-based sensing of heavy metal ions

The adsorption performance of ions onto the CelloZIFPaper offers further use for electrochemical sensing (**Fig. 7**). Electrochemical measurements reveal significant changes in the current output of CelloZIFPaper upon metal adsorption (**Figure S14**). Thus, CelloZIFPaper can be used as an electrode for metal detection. The preparation of the electrode is simple. CelloZIFPaper, prepared both with the *ex-situ* and the *in-situ* procedure 1:0.5 and 1:4 ratio (selected as a reference due to their ZIF content), were cut into rectangular-shaped pieces ($1 \times 2 \text{ cm}^2$). Then, aqueous solutions of the metal ions (Co^{2+} , Cu^{2+} , Fe^{3+} , Cd^{2+} , and Pb^{2+}) were poured dropwise on the electrodes and dried before immersing them into an electrolyte solution (**Fig. 7**). The electrochemical measurements such as CV and LSV were conducted (**Fig. 8**).

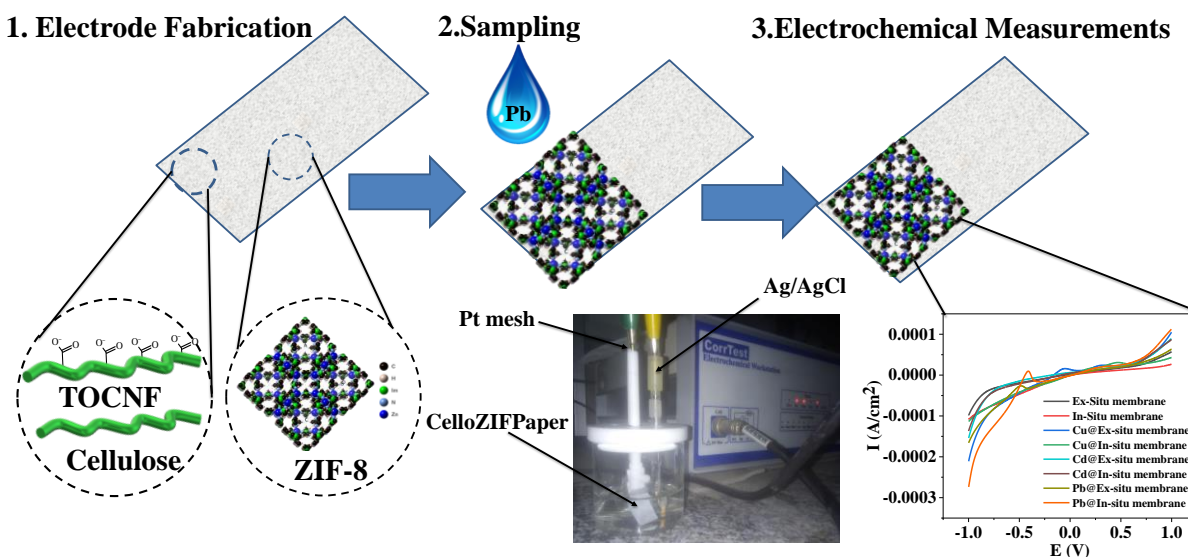


FIGURE 7 Schematic representation of electrode fabrication, sampling, and electrochemical measurements of CelloZIFPaper. The inset camera image shows the setup of the cell electrodes and potentiostat.

CV curves of CelloZIFPaper-based electrodes using *ex-situ* and *in-situ* procedures with and without metal ions adsorption are shown in **Fig. 8a-b**. The data analysis reveals changes in the output current of the CelloZIFPaper electrode upon interaction with the metal ions (**Fig. 8a-b**).

The CelloZIFPaper electrode shows a significant shift in both current outputs, i.e., the anodic and cathodic, after the adsorption of metal ions. The adsorbed Pb^{2+} ions show the most remarkable current output change, revealing high selectivity. The high selectivity of the CelloZIFPaper electrode toward Pb^{2+} is mainly due to the precipitation as insoluble PbSO_4 . Tetrahedral metal ions such as Cu^{2+} and Co^{2+} ions can coordinate with Zn metal ions inside ZIF frameworks. These interactions are further supported by the potentiodynamic polarization test (PD, **Figure S15**). There is an apparent anodic and cathodic polarization after the adsorption of metal ions. The shift toward positive potential, i.e., anodic polarization, of CelloPaper after adding ZIF indicates the possibility of electrons withdrawing from the electrode. There is a significant cathodic polarization (the working electrode becomes more negative) after the adsorption of Co^{2+} ions. These observations indicate that CelloZIFPaper can be used as a working electrode for electrochemical-base sensing of metal ions (**Fig. 8c**).

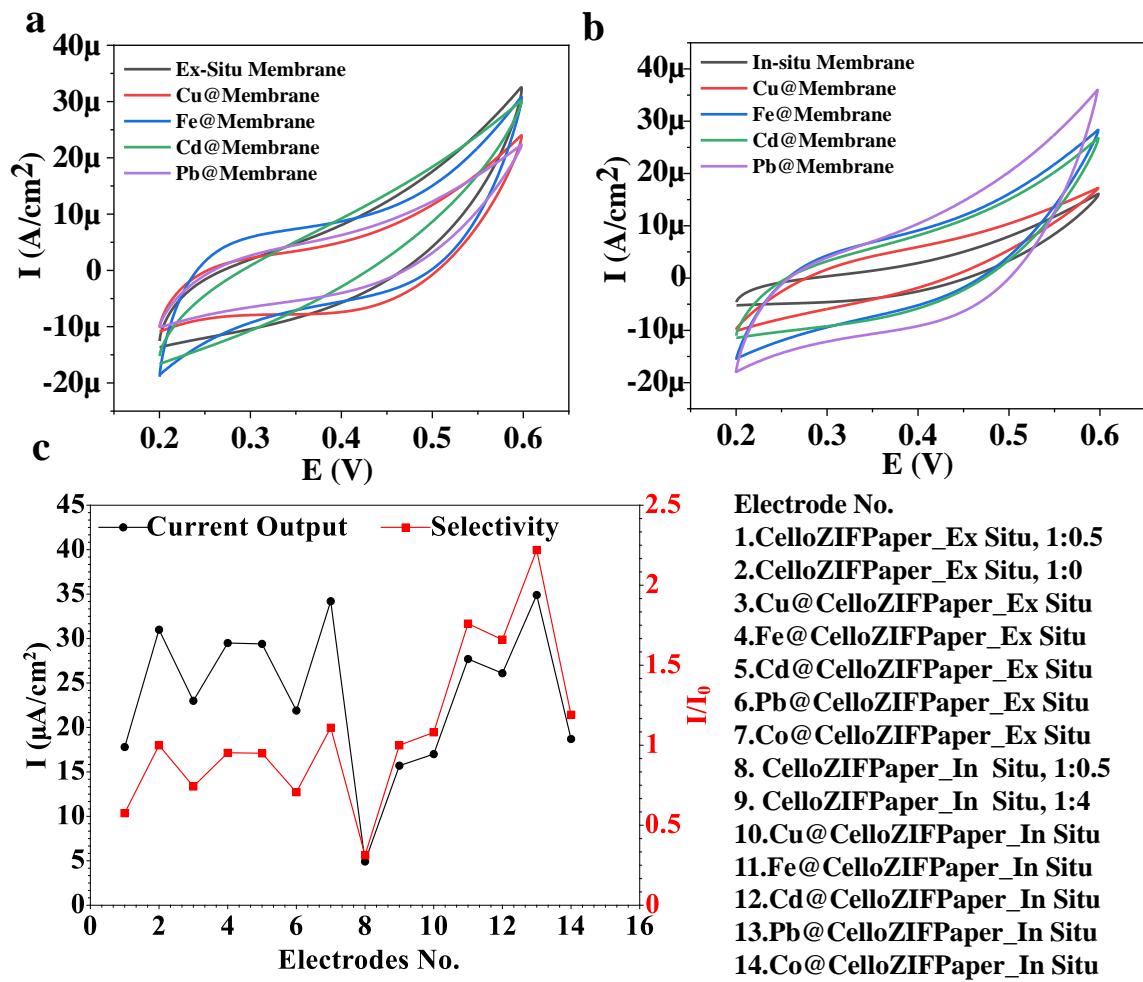


FIGURE 8 a-b) CV for CelloZIFPaper electrode before and after metal adsorption for a) CelloZIFPaper_Ex Situ and b) CelloZIFPaper_In Situ, and c) output current of CelloZIFPaper electrode after metal ions adsorption.

LSV measurements of CelloZIFPaper before and after metal ions deposition were recorded (**Fig. 9**). The output current of CelloZIFPaper shows changes upon interaction with different metals. Based on the relative output current of the CelloZIFPaper electrode, there is high selectivity toward Pb^{2+} compared to the other investigated metal ion species (**Fig. 8d**). Furthermore, there is a reduction peak at a potential of -0.47 V for Pb^{2+} absent for other metal ions. These observations reveal that the CelloZIFPaper electrode can be used to detect Pb^{2+} ions using electrochemical-based sensing. Paper interaction with different concentrations of Pb^{2+} was also recorded using LSV

(Fig. 9). CelloZIFPaper electrodes show a limit of detection (LOD) of 40 μM and 8 μM for membranes synthesized via *ex-situ* (Fig. 9a) and *in-situ* (Fig. 9b) procedures, respectively. CelloZIFPaper_ In Situ electrodes exhibited higher sensitivity toward Pb^{2+} than CelloZIFPaper_ Ex Situ electrodes. The electrode shows a linear relationship in the concentration range of 8-40 μM ($R^2 = 0.95$, Fig. 9c).

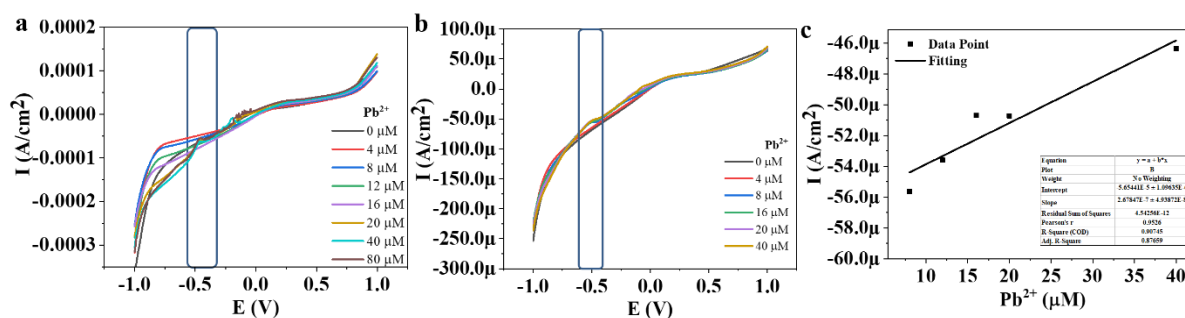


FIGURE 9 a-b) LSV upon interactions with different concentrations of Pb^{2+} using CelloZIFPaper electrode prepared using a) *Ex-situ* and b) *In-situ* procedure, and c) linear relationship.

Various ZIF-based materials have been used for electrochemical-based sensing. A comparative study among some of them is presented in **Table 3**. The use of CelloZIFPaper as a working electrode is cheaper than conventional electrodes such as glassy carbon electrodes (GCE) [81] or gold (Au) electrodes (AE) for selective detection of Hg^{2+} ions [82]. CelloZIFPaper-based electrodes exhibit good current stability using the chronoamperometry test (**Figure S16**). The presence of active sites such as nitrogen pyridinic-N and pyrrolic-N with two unpaired electrons acted as additional adsorption sites for metal ions [83]. CelloZIFPaper can be used directly without carbonizing ZIF-8 to ZnO@C or deposition of other nanomaterials [81]. It can be used directly without the need for binding or conductive materials. The electrode fabrication is simple and requires no tedious efforts [55]. In addition, the presence of cellulose functional groups (-OH and -COOH) in CelloZIFPaper enhances the metal adsorption making it a good candidate for the electrochemical sensing of, for instance, Pb^{2+} (**Table 3**).

Several carbohydrate polymers were reported for ZIF-based electrodes, including the use of β -cyclodextrin (β -CD) [84] and chitosan [85]. ZIF-8@dimethylglyoxime/ β -cyclodextrin/reduced graphene oxide (ZIF-8@DMG/ β -CD/RGO) was reported for electrochemical sensing of Ni^{2+} using **differential pulse adsorptive stripping voltammetry (DP AdSV, Table 3)** [84]. CelloZIFPaper was used without the need for GCE or chelating agents such as DMG, β -CD, or rGO [84]. Zn/Ni-ZIF-8/Carbon black (XC-72)/Nafion/GCE was used for the detection of Pb^{2+} and Cu^{2+} using **differential pulse voltammetry (DPV, Table 3)** [86]. It showed good selectivity towards both of the studied metal ions based on each species' reduction potential [86]. However, the electrode preparation is tedious and suffers from particle aggregation. ZIF8-derived Ag@Au core-shell nanoparticles (Ag@Au/ZIF-8) were modified with an aptasensor modifier and loaded into AE for successful selective detection of Hg^{2+} [82]. However, electrode fabrication requires expensive chemical reagents.

Table 3 A comparison among different ZIF-based materials for heavy metal sensing.

Materials	Electrode	Methods	Metals	Linear range	LOD	Selectivity	Ref.
ZIF-8@DMG/ β -CD/RGO	GCE	DP AdSV	Ni ²⁺	0.01–1.0 μ M	0.005 μ M	Yes	[84]
Zn/Ni-ZIF-8/XC-72/Nafion/GCE	GCE	DPV	Pb ²⁺ Cu ²⁺	0.794–39.6 ppm 0.397–19.9 ppm	0.0150 ppm 0.0096 ppm	Yes	[86]
H-ZnO@NC/Nafion/GCE	GCE	DPASV	Cd ²⁺	0.3–300 μ g L ⁻¹	0.1 μ g L ⁻¹	Yes	[83]
Ag@Au/ZIF-8/AE	Au electrode	DPV EIS	Hg ²⁺	1×10^{-16} – 1×10^{-12} M (DPV) 5×10^{-15} – 1×10^{-12} M (EIS)	1.8×10^{-17} M 1.3×10^{-16} M	Yes	[82]
ZIF-8-CS/GCE	GCE	DPASV	Hg ²⁺ Cu ²⁺ Pb ²⁺ Cd ²⁺	1–80 μ M 1–100 μ M 1–100 μ M 1–100 μ M	0.0293 μ M 0.108 μ M 0.0619 μ M 0.135 μ M	No	[85]
CelloZIFPaper	Self-standing	LSV	Pb ²⁺	8–40 μ M	8 μ M	Yes	This Work

Conclusions

Simple and water-based methods were reported for processing cellulose-ZIF-8 hybrids into paper sheets with a diameter of 200 mm. Cellulose is an excellent substrate material for the growth of ZIF-8 due to its abundant functional groups, i.e., -OH, -C=O, and -COOH. Two routes, namely *in-situ* and *ex-situ*, were devised to grow ZIF-8 onto TOCNF and CP, with the ZIF-8 crystalline structure preserved in both cases. The properties and performance of the CelloZIFPaper prepared via *in-situ* procedure are consistently better than the ones prepared via *ex-situ* procedure. The CelloZIF paper hybrids combine ion exchange and interparticle diffusion of MOFs with electrostatic interaction and network forming capabilities of carboxylated nanocellulose. The sheets exhibited high performance (adsorption capacities of 66.2-354.0 mg/g) towards adsorption and electrochemical-based sensing of heavy metal ions. The electrochemical-based method using CelloZIFPaper is promising as a lab-on-paper application for label-free detection of heavy metal ions in aqueous solutions. CelloZIFPaper could potentially be used for related applications, for instance, the adsorption of volatile organic compounds and toxic gases.

Data availability

All experimental data used in this study are available for interested readers upon communication with the corresponding author.

CRedit authorship contribution statement

Hani Nasser Abdelhamid: Conceptualization, methodology, characterization, resources, data collection and analysis, visualization, and writing of the original manuscript. **Dimitrios Georgouvelas:** characterization, data collection and analysis, writing and editing of the manuscript. **Ulrica Edlund:** Validation, supervision, review, and edit of manuscript, funding

acquisition. **Aji Mathew:** Conceptualization, methodology, validation, supervision, resources, review and edit of the manuscript, project administration, funding acquisition.

Declaration of Competing Interest

The authors declare no competing financial or any other sort of interest that may influence the work presented in this study.

Acknowledgments

This project is funded by The Swedish Foundation for Strategic Environmental Research (Mistra), project name MISTRA TerraClean (project no. 2015/31).

Conflict of Interest

The authors declare no conflict of interest.

References

- [1] M. Ibrahim, H.N. Abdelhamid, A.M. Abuelftooh, S.G. Mohamed, Z. Wen, X. Sun, Covalent Organic Frameworks-Derived Nitrogen-Doped Carbon/Reduced Graphene Oxide as Electrodes for Supercapacitor, *SSRN Electron. J.* (2022). <https://doi.org/10.2139/ssrn.4063571>.
- [2] A.R. Abdellah, H.N. Abdelhamid, A.-B.A.A.M. El-Adasy, A.A. Atalla, K.I. Aly, One-pot synthesis of hierarchical porous covalent organic frameworks and two-dimensional nanomaterials for selective removal of anionic dyes, *J. Environ. Chem. Eng.* 8 (2020) 104054. <https://doi.org/10.1016/j.jece.2020.104054>.
- [3] A.F. Abdel-Magied, H.N. Abdelhamid, R.M. Ashour, L. Fu, M. Dowaidar, W. Xia, K. Forsberg, Magnetic Metal-Organic Frameworks for Efficient Removal of Cadmium(II), and Lead(II) from Aqueous Solution, *J. Environ. Chem. Eng.* (2022) 107467. <https://doi.org/10.1016/j.jece.2022.107467>.
- [4] A.I.A. Soliman, H.N. Abdelhamid, Aboel-Magd A. Abdel-Wahab Assiut University, Hierarchical Porous Zeolitic Imidazolate Frameworks (ZIF-8) and ZnO@N-doped Carbon for Selective Adsorption and Photocatalytic Degradation of Organic Pollutants, *ChemRxiv. Cambridge Cambridge Open Engag.* 2022; (2022). <https://doi.org/10.26434/chemrxiv-2022-rwvtp>.
- [5] H.N. Abdelhamid, G.A.-E. Mahmoud, W. Sharmouk, W. Sharmoukh, Correction: A cerium-based MOFzyme with multi-enzyme-like activity for the disruption and inhibition of fungal recolonization, *J. Mater. Chem. B.* 8 (2020) 7557–7557. <https://doi.org/10.1039/D0TB90139C>.

- [6] H.N. Abdelhamid, G.A.-E. Mahmoud, W. Sharmouk, A cerium-based MOFzyme with multi-enzyme-like activity for the disruption and inhibition of fungal recolonization, *J. Mater. Chem. B.* 8 (2020) 7548–7556. <https://doi.org/10.1039/D0TB00894J>.
- [7] H.N. Abdelhamid, UiO-66 as a catalyst for hydrogen production via the hydrolysis of sodium borohydride, *Dalt. Trans.* 49 (2020) 10851–10857. <https://doi.org/10.1039/D0DT01688H>.
- [8] M.N. Goda, H.N. Abdelhamid, A.E.-A.A. Said, Zirconium Oxide Sulfate-Carbon (ZrOSO₄@C) Derived from Carbonized UiO-66 for Selective Production of Dimethyl Ether, *ACS Appl. Mater. Interfaces.* 12 (2020) 646–653. <https://doi.org/10.1021/acsami.9b17520>.
- [9] A.A. Kassem, H.N. Abdelhamid, D.M. Fouad, S.A. Ibrahim, Metal-organic frameworks (MOFs) and MOFs-derived CuO@C for hydrogen generation from sodium borohydride, *Int. J. Hydrogen Energy.* 44 (2019) 31230–31238. <https://doi.org/10.1016/j.ijhydene.2019.10.047>.
- [10] H.N. Abdelhamid, M. Dowaidar, M. Hällbrink, Ü. Langel, Cell Penetrating Peptides-Hierarchical Porous Zeolitic Imidazolate Frameworks Nanoparticles: An Efficient Gene Delivery Platform, *SSRN Electron. J.* (2019). <https://doi.org/10.2139/ssrn.3435895>.
- [11] H.N. Abdelhamid, Surfactant assisted synthesis of hierarchical porous metal-organic frameworks nanosheets, *Nanotechnology.* 30 (2019) 435601. <https://doi.org/10.1088/1361-6528/ab30f6>.
- [12] H.N. Abdelhamid, Lanthanide Metal-Organic Frameworks and Hierarchical Porous Zeolitic Imidazolate Frameworks: Synthesis, Properties, and Applications, Stockholm University, Faculty of Science, 2017. <https://doi.org/oai:DiVA.org:su-146398>.
- [13] A.I.A. Soliman, A.-M.A. Abdel-Wahab, H.N. Abdelhamid, Hierarchical porous zeolitic imidazolate frameworks (ZIF-8) and ZnO@N-doped carbon for selective adsorption and photocatalytic degradation of organic pollutants, *RSC Adv.* 12 (2022) 7075–7084. <https://doi.org/10.1039/D2RA00503D>.
- [14] M.N. Goda, A.E.-A.A. Said, H.N. Abdelhamid, Highly selective dehydration of methanol over metal-organic frameworks (MOFs)-derived ZnO@Carbon, *J. Environ. Chem. Eng.* 9 (2021) 106336. <https://doi.org/10.1016/j.jece.2021.106336>.
- [15] H.N. Abdelhamid, Solid Acid Zirconium Oxo Sulfate/Carbon-Derived UiO-66 for Hydrogen Production, *Energy & Fuels.* 35 (2021) 10322–10326. <https://doi.org/10.1021/acs.energyfuels.1c00516>.
- [16] A.A. Kassem, H.N. Abdelhamid, D.M. Fouad, S.A. Ibrahim, Catalytic reduction of 4-nitrophenol using copper terephthalate frameworks and CuO@C composite, *J. Environ. Chem. Eng.* 9 (2021) 104401. <https://doi.org/10.1016/j.jece.2020.104401>.
- [17] H.N. Abdelhamid, High performance and ultrafast reduction of 4-nitrophenol using metal-organic frameworks, *J. Environ. Chem. Eng.* 9 (2021) 104404. <https://doi.org/10.1016/j.jece.2020.104404>.
- [18] H.N. Abdelhamid, W. Sharmoukh, Intrinsic catalase-mimicking MOFzyme for sensitive detection of hydrogen peroxide and ferric ions, *Microchem. J.* 163 (2021) 105873. <https://doi.org/10.1016/j.microc.2020.105873>.
- [19] H.N. Abdelhamid, M.N. Goda, A.E.-A.A. Said, Selective dehydrogenation of isopropanol on carbonized metal-organic frameworks, *Nano-Structures & Nano-Objects.* 24 (2020) 100605. <https://doi.org/10.1016/j.nanoso.2020.100605>.
- [20] A.A. Kassem, H.N. Abdelhamid, D.M. Fouad, S.A. Ibrahim, Hydrogenation reduction of

- dyes using metal-organic framework-derived CuO@C, *Microporous Mesoporous Mater.* 305 (2020) 110340. <https://doi.org/10.1016/j.micromeso.2020.110340>.
- [21] X. Ren, G. Liao, Z. Li, H. Qiao, Y. Zhang, X. Yu, B. Wang, H. Tan, L. Shi, X. Qi, H. Zhang, Two-dimensional MOF and COF nanosheets for next-generation optoelectronic applications, *Coord. Chem. Rev.* 435 (2021) 213781. <https://doi.org/10.1016/j.ccr.2021.213781>.
- [22] M.-X. Wu, Y. Wang, G. Zhou, X. Liu, Sparks from different worlds: Collaboration of MOFs and COFs, *Coord. Chem. Rev.* 430 (2021) 213735. <https://doi.org/10.1016/j.ccr.2020.213735>.
- [23] C. Liu, J. Wang, J. Wan, C. Yu, MOF-on-MOF hybrids: Synthesis and applications, *Coord. Chem. Rev.* 432 (2021) 213743. <https://doi.org/10.1016/j.ccr.2020.213743>.
- [24] X. Zhang, Z. Wang, M. Ding, Y. Feng, J. Yao, Advances in cellulose-metal organic framework composites: Preparation and application, *J. Mater. Chem. A.* (2021). <https://doi.org/10.1039/D1TA06468A>.
- [25] X. Liu, Y. Xiao, Z. Zhang, Z. You, J. Li, D. Ma, B. Li, Recent progress in metal organic frameworks@cellulose hybrids and their applications, *Chinese J. Chem.* (2021) cjoc.202100534. <https://doi.org/10.1002/cjoc.202100534>.
- [26] H.N. Abdelhamid, A. Mathew, Cellulose-Metal Organic Frameworks (CelloMOFs) Hybrid Materials and their Multifaceted Applications: A Review, *Coord. Chem. Rev.* 451 (2022) 214263. <https://doi.org/10.1016/j.ccr.2021.214263>.
- [27] H.N. Abdelhamid, S.A. Al Kiey, W. Sharmoukh, A high-performance hybrid supercapacitor electrode based on ZnO/nitrogen-doped carbon nanohybrid, *Appl. Organomet. Chem.* (2021). <https://doi.org/10.1002/aoc.6486>.
- [28] H.N. Abdelhamid, Zeolitic Imidazolate Frameworks (ZIF-8) for Biomedical Applications: A Review, *Curr. Med. Chem.* 28 (2021) 7023–7075. <https://doi.org/10.2174/0929867328666210608143703>.
- [29] H.N. Abdelhamid, *Advanced Functional Porous Materials*, Springer International Publishing, Cham, 2022. <https://doi.org/10.1007/978-3-030-85397-6>.
- [30] H.M. El-Bery, H.N. Abdelhamid, Photocatalytic hydrogen generation via water splitting using ZIF-67 derived Co₃O₄@C/TiO₂, *J. Environ. Chem. Eng.* 9 (2021) 105702. <https://doi.org/10.1016/j.jece.2021.105702>.
- [31] H.N. Abdelhamid, Zeolitic imidazolate frameworks (ZIF-8, ZIF-67, and ZIF-L) for hydrogen production, *Appl. Organomet. Chem.* 35 (2021) e6319. <https://doi.org/10.1002/aoc.6319>.
- [32] H.N. Abdelhamid, Biointerface between ZIF-8 and biomolecules and their applications, *Biointerface Res. Appl. Chem.* 11 (2021) 8283–8297. <https://doi.org/10.33263/BRIAC111.82838297>.
- [33] H.N. Abdelhamid, Dye encapsulated hierarchical porous zeolitic imidazolate frameworks for carbon dioxide adsorption, *J. Environ. Chem. Eng.* 8 (2020) 104008. <https://doi.org/10.1016/j.jece.2020.104008>.
- [34] H.N. Abdelhamid, M. Dowaidar, Ü. Langel, Carbonized chitosan encapsulated hierarchical porous zeolitic imidazolate frameworks nanoparticles for gene delivery, *Microporous Mesoporous Mater.* 302 (2020) 110200. <https://doi.org/10.1016/j.micromeso.2020.110200>.
- [35] H.N. Abdelhamid, M. Dowaidar, M. Hällbrink, Ü. Langel, Gene delivery using cell penetrating peptides-zeolitic imidazolate frameworks, *Microporous Mesoporous Mater.*

- 300 (2020) 110173. <https://doi.org/10.1016/j.micromeso.2020.110173>.
- [36] H.N. Abdelhamid, Salts Induced Formation of Hierarchical Porous ZIF-8 and Their Applications for CO₂ Sorption and Hydrogen Generation via NaBH₄ Hydrolysis, *Macromol. Chem. Phys.* 221 (2020) 2000031. <https://doi.org/10.1002/macp.202000031>.
- [37] H.N. Abdelhamid, Hierarchical porous ZIF-8 for hydrogen production via the hydrolysis of sodium borohydride, *Dalt. Trans.* 49 (2020) 4416–4424. <https://doi.org/10.1039/D0DT00145G>.
- [38] H.N. Abdelhamid, A.M. El-Zohry, J. Cong, T. Thersleff, M. Karlsson, L. Kloo, X. Zou, Towards implementing hierarchical porous zeolitic imidazolate frameworks in dye-sensitized solar cells, *R. Soc. Open Sci.* 6 (2019) 190723. <https://doi.org/10.1098/rsos.190723>.
- [39] A.F. Abdel-Magied, H.N. Abdelhamid, R.M. Ashour, X. Zou, K. Forsberg, Hierarchical porous zeolitic imidazolate frameworks nanoparticles for efficient adsorption of rare-earth elements, *Microporous Mesoporous Mater.* 278 (2019) 175–184. <https://doi.org/10.1016/j.micromeso.2018.11.022>.
- [40] S. Sultan, H.N. Abdelhamid, X. Zou, A.P. Mathew, CelloMOF: Nanocellulose Enabled 3D Printing of Metal-Organic Frameworks, *Adv. Funct. Mater.* (2018) 1805372. <https://doi.org/10.1002/adfm.201805372>.
- [41] H.N. Abdelhamid, A.P. Mathew, A Review on Cellulose-based Materials for Biomedicine, *Preprints.* (2022) 2022010035. <https://doi.org/10.20944/preprints202201.0035.v1>.
- [42] L. Valencia, H.N. Abdelhamid, Nanocellulose leaf-like zeolitic imidazolate framework (ZIF-L) foams for selective capture of carbon dioxide, *Carbohydr. Polym.* 213 (2019) 338–345. <https://doi.org/10.1016/j.carbpol.2019.03.011>.
- [43] R.M. Rego, G. Kuriya, M.D. Kurkuri, M. Kigga, MOF based engineered materials in water remediation: Recent trends, *J. Hazard. Mater.* (2020) 123605. <https://doi.org/10.1016/j.jhazmat.2020.123605>.
- [44] H.N. Abdelhamid, A.P. Mathew, In-situ growth of zeolitic imidazolate frameworks into a cellulosic filter paper for the reduction of 4-nitrophenol, *Carbohydr. Polym.* 274 (2021) 118657. <https://doi.org/10.1016/j.carbpol.2021.118657>.
- [45] H.N. Abdelhamid, A.P. Mathew, Cellulose-Based Materials for Water Remediation: Adsorption, Catalysis, and Antifouling, *Front. Chem. Eng.* 3 (2021) 790314. <https://doi.org/10.3389/fceng.2021.790314>.
- [46] S. Zhou, V. Apostolopoulou-Kalkavoura, M.V. Tavares da Costa, L. Bergström, M. Strømme, C. Xu, Elastic Aerogels of Cellulose Nanofibers@Metal–Organic Frameworks for Thermal Insulation and Fire Retardancy, *Nano-Micro Lett.* 12 (2020) 9. <https://doi.org/10.1007/s40820-019-0343-4>.
- [47] J. Dhainaut, M. Bonneau, R. Ueoka, K. Kanamori, S. Furukawa, Formulation of Metal–Organic Framework Inks for the 3D Printing of Robust Microporous Solids toward High-Pressure Gas Storage and Separation, *ACS Appl. Mater. Interfaces.* 12 (2020) 10983–10992. <https://doi.org/10.1021/acsami.9b22257>.
- [48] H. Zhu, X. Yang, E.D. Cranston, S. Zhu, Flexible and Porous Nanocellulose Aerogels with High Loadings of Metal-Organic-Framework Particles for Separations Applications, *Adv. Mater.* 28 (2016) 7652–7657. <https://doi.org/10.1002/adma.201601351>.
- [49] X. Ma, Y. Lou, X.-B. Chen, Z. Shi, Y. Xu, Multifunctional flexible composite aerogels constructed through in-situ growth of metal-organic framework nanoparticles on bacterial

- cellulose, *Chem. Eng. J.* 356 (2019) 227–235. <https://doi.org/10.1016/j.cej.2018.09.034>.
- [50] M. Matsumoto, T. Kitaoka, Ultraselective Gas Separation by Nanoporous Metal–Organic Frameworks Embedded in Gas-Barrier Nanocellulose Films, *Adv. Mater.* 28 (2016) 1765–1769. <https://doi.org/10.1002/adma.201504784>.
- [51] C. Shen, Z. Mao, H. Xu, L. Zhang, Y. Zhong, B. Wang, X. Feng, C. Tao, X. Sui, Catalytic MOF-loaded cellulose sponge for rapid degradation of chemical warfare agents simulant, *Carbohydr. Polym.* 213 (2019) 184–191. <https://doi.org/10.1016/j.carbpol.2019.02.044>.
- [52] J. Rostami, K. Gordeyeva, T. Benselfelt, E. Lahchaichi, S.A. Hall, A. V. Riazanova, P.A. Larsson, G. Cinar Ciftci, L. Wågberg, Hierarchical build-up of bio-based nanofibrous materials with tunable metal–organic framework biofunctionality, *Mater. Today*. (2021). <https://doi.org/10.1016/j.mattod.2021.04.013>.
- [53] ATSDR, Substance Priority List | ATSDR, Agency Toxic Subst. Dis. Regist. (2017) 1–11. <https://www.atsdr.cdc.gov/spl/index.html#2019spl> (accessed September 1, 2021).
- [54] R. Jain, A. Thakur, P. Kaur, K.-H. Kim, P. Devi, Advances in imaging-assisted sensing techniques for heavy metals in water: Trends, challenges, and opportunities, *TrAC Trends Anal. Chem.* 123 (2020) 115758. <https://doi.org/10.1016/j.trac.2019.115758>.
- [55] H. Sohrabi, A. Khataee, S. Ghasemzadeh, M.R. Majidi, Y. Orooji, Layer double hydroxides (LDHs)- based electrochemical and optical sensing assessments for quantification and identification of heavy metals in water and environment samples: A review of status and prospects, *Trends Environ. Anal. Chem.* 31 (2021) e00139. <https://doi.org/10.1016/j.teac.2021.e00139>.
- [56] J. Yao, H. Wang, Zeolitic imidazolate framework composite membranes and thin films: synthesis and applications, *Chem. Soc. Rev.* 43 (2014) 4470. <https://doi.org/10.1039/c3cs60480b>.
- [57] A. Isogai, T. Saito, H. Fukuzumi, TEMPO-oxidized cellulose nanofibers, *Nanoscale*. 3 (2011) 71–85. <https://doi.org/10.1039/c0nr00583e>.
- [58] H.N. Abdelhamid, Z. Huang, A.M. El-Zohry, H. Zheng, X. Zou, A Fast and Scalable Approach for Synthesis of Hierarchical Porous Zeolitic Imidazolate Frameworks and One-Pot Encapsulation of Target Molecules, *Inorg. Chem.* 56 (2017) 9139–9146. <https://doi.org/10.1021/acs.inorgchem.7b01191>.
- [59] S. Brunauer, P.H. Emmett, E. Teller, Adsorption of Gases in Multimolecular Layers, *J. Am. Chem. Soc.* 60 (1938) 309–319. <https://doi.org/10.1021/ja01269a023>.
- [60] I. Langmuir, THE ADSORPTION OF GASES ON PLANE SURFACES OF GLASS, MICA AND PLATINUM., *J. Am. Chem. Soc.* 40 (1918) 1361–1403. <https://doi.org/10.1021/ja02242a004>.
- [61] J. Tauc, Optical properties and electronic structure of amorphous Ge and Si, *Mater. Res. Bull.* 3 (1968) 37–46. [https://doi.org/10.1016/0025-5408\(68\)90023-8](https://doi.org/10.1016/0025-5408(68)90023-8).
- [62] H.N. Abdelhamid, X. Zou, Template-free and room temperature synthesis of hierarchical porous zeolitic imidazolate framework nanoparticles and their dye and CO₂ sorption, *Green Chem.* 20 (2018) 1074–1084. <https://doi.org/10.1039/c7gc03805d>.
- [63] X. Ju, M. Bowden, E.E. Brown, X. Zhang, An improved X-ray diffraction method for cellulose crystallinity measurement, *Carbohydr. Polym.* 123 (2015) 476–481. <https://doi.org/10.1016/j.carbpol.2014.12.071>.
- [64] H. Dai, X. Yuan, L. Jiang, H. Wang, J. Zhang, J. Zhang, T. Xiong, Recent advances on ZIF-8 composites for adsorption and photocatalytic wastewater pollutant removal: Fabrication, applications and perspective, *Coord. Chem. Rev.* 441 (2021) 213985.

- <https://doi.org/10.1016/j.ccr.2021.213985>.
- [65] J. Wen, X. Hu, Metal selectivity and effects of co-existing ions on the removal of Cd, Cu, Ni, and Cr by ZIF-8-EGCG nanoparticles, *J. Colloid Interface Sci.* 589 (2021) 578–586. <https://doi.org/10.1016/j.jcis.2021.01.021>.
- [66] D. Georgouvelas, H.N. Abdelhamid, J. Li, U. Edlund, A.P. Mathew, All-cellulose functional membranes for water treatment: Adsorption of metal ions and catalytic decolorization of dyes, *Carbohydr. Polym.* 264 (2021) 118044. <https://doi.org/10.1016/j.carbpol.2021.118044>.
- [67] H. Nasser Abdelhamid, A.P. Mathew, Cellulose-zeolitic imidazolate frameworks (CelloZIFs) for multifunctional environmental remediation: Adsorption and catalytic degradation, *Chem. Eng. J.* 426 (2021) 131733. <https://doi.org/10.1016/j.cej.2021.131733>.
- [68] C. Chizallet, S. Lazare, D. Bazer-Bachi, F. Bonnier, V. Lecocq, E. Soyer, A.-A. Quoineaud, N. Bats, Catalysis of Transesterification by a Nonfunctionalized Metal–Organic Framework: Acido-Basicity at the External Surface of ZIF-8 Probed by FTIR and ab Initio Calculations, *J. Am. Chem. Soc.* 132 (2010) 12365–12377. <https://doi.org/10.1021/ja103365s>.
- [69] L. Valencia, S. Kumar, E.M. Nomena, G. Salazar-Alvarez, A.P. Mathew, In-Situ Growth of Metal Oxide Nanoparticles on Cellulose Nanofibrils for Dye Removal and Antimicrobial Applications, *ACS Appl. Nano Mater.* (2020) acsanm.0c01511. <https://doi.org/10.1021/acsanm.0c01511>.
- [70] Y. Zhang, Z. Xie, Z. Wang, X. Feng, Y. Wang, A. Wu, Unveiling the adsorption mechanism of zeolitic imidazolate framework-8 with high efficiency for removal of copper ions from aqueous solutions, *Dalt. Trans.* 45 (2016) 12653–12660. <https://doi.org/10.1039/C6DT01827K>.
- [71] S. Yang, L. Peng, O.A. Syzgantseva, O. Trukhina, I. Kochetygov, A. Justin, D.T. Sun, H. Abedini, M.A. Syzgantseva, E. Oveisi, G. Lu, W.L. Queen, Preparation of Highly Porous Metal–Organic Framework Beads for Metal Extraction from Liquid Streams, *J. Am. Chem. Soc.* 142 (2020) 13415–13425. <https://doi.org/10.1021/jacs.0c02371>.
- [72] J. Li, Q. Duan, Z. Wu, X. Li, K. Chen, G. Song, A. Alsaedi, T. Hayat, C. Chen, Few-layered metal-organic framework nanosheets as a highly selective and efficient scavenger for heavy metal pollution treatment, *Chem. Eng. J.* 383 (2020) 123189. <https://doi.org/10.1016/j.cej.2019.123189>.
- [73] R. Xu, M. Jian, Q. Ji, C. Hu, C. Tang, R. Liu, X. Zhang, J. Qu, 2D water-stable zinc-benzimidazole framework nanosheets for ultrafast and selective removal of heavy metals, *Chem. Eng. J.* 382 (2020) 122658. <https://doi.org/10.1016/j.cej.2019.122658>.
- [74] F. Yang, M. Du, K. Yin, Z. Qiu, J. Zhao, C. Liu, G. Zhang, Y. Gao, H. Pang, Applications of Metal-Organic Frameworks in Water Treatment: A Review, *Small.* (2021) 2105715. <https://doi.org/10.1002/sml.202105715>.
- [75] Y. Liu, H. Pang, X. Wang, S. Yu, Z. Chen, P. Zhang, L. Chen, G. Song, N. Saleh Alharbi, S. Omar Rabah, X. Wang, Zeolitic imidazolate framework-based nanomaterials for the capture of heavy metal ions and radionuclides: A review, *Chem. Eng. J.* 406 (2021) 127139. <https://doi.org/10.1016/j.cej.2020.127139>.
- [76] Y. Huang, X. Zeng, L. Guo, J. Lan, L. Zhang, D. Cao, Heavy metal ion removal of wastewater by zeolite-imidazolate frameworks, *Sep. Purif. Technol.* 194 (2018) 462–469. <https://doi.org/10.1016/j.seppur.2017.11.068>.
- [77] D. Li, F. Xu, Removal of Cu (II) from aqueous solutions using ZIF-8@GO composites, *J.*

- Solid State Chem. 302 (2021) 122406. <https://doi.org/10.1016/j.jssc.2021.122406>.
- [78] X. Jiang, S. Su, J. Rao, S. Li, T. Lei, H. Bai, S. Wang, X. Yang, Magnetic metal-organic framework (Fe₃O₄@ZIF-8) core-shell composite for the efficient removal of Pb(II) and Cu(II) from water, *J. Environ. Chem. Eng.* 9 (2021) 105959. <https://doi.org/10.1016/j.jece.2021.105959>.
- [79] L. Peng, X. Zhang, Y. Sun, Y. Xing, C. Li, Heavy metal elimination based on metal organic framework highly loaded on flexible nanofibers, *Environ. Res.* 188 (2020) 109742. <https://doi.org/10.1016/j.envres.2020.109742>.
- [80] D.N. binti Awang Chee, F. Aziz, A.F. Ismail, M.A. bin Mohamed Amin, M.S. Abdullah, Dual-function ZIF-8 membrane supported on alumina hollow fiber membrane for copper(II) removal, *J. Environ. Chem. Eng.* 9 (2021) 105343. <https://doi.org/10.1016/j.jece.2021.105343>.
- [81] M. Hu, X. Hu, Y. Zhang, M. Teng, R. Deng, G. Xing, J. Tao, G. Xu, J. Chen, Y. Zhang, G. Zhang, Label-free electrochemical immunosensor based on AuNPs/Zn/Ni-ZIF-8-800@graphene composites for sensitive detection of monensin in milk, *Sensors Actuators B Chem.* 288 (2019) 571–578. <https://doi.org/10.1016/j.snb.2019.03.014>.
- [82] N. Salandari-Jolge, A.A. Ensafi, B. Rezaei, Ultra-sensitive electrochemical aptasensor based on zeolitic imidazolate framework-8 derived Ag/Au core-shell nanoparticles for mercury detection in water samples, *Sensors Actuators B Chem.* 331 (2021) 129426. <https://doi.org/10.1016/j.snb.2020.129426>.
- [83] X. Zhang, Q. Wang, J. Li, L. Huang, D. Yu, S. Dong, In situ fabrication of hollow ZnO@NC polyhedra from ZIF-8 for the determination of trace Cd(ii), *Analyst.* 143 (2018) 2837–2843. <https://doi.org/10.1039/C8AN00515J>.
- [84] X. Cui, B. Yang, S. Zhao, X. Li, M. Qiao, R. Mao, Y. Wang, X. Zhao, Electrochemical sensor based on ZIF-8@dimethylglyoxime and β-cyclodextrin modified reduced graphene oxide for nickel (II) detection, *Sensors Actuators B Chem.* 315 (2020) 128091. <https://doi.org/10.1016/j.snb.2020.128091>.
- [85] Y. Chu, F. Gao, F. Gao, Q. Wang, Enhanced stripping voltammetric response of Hg²⁺, Cu²⁺, Pb²⁺ and Cd²⁺ by ZIF-8 and its electrochemical analytical application, *J. Electroanal. Chem.* 835 (2019) 293–300. <https://doi.org/10.1016/j.jelechem.2019.01.053>.
- [86] D. Li, X. Qiu, H. Guo, D. Duan, W. Zhang, J. Wang, J. Ma, Y. Ding, Z. Zhang, A simple strategy for the detection of Pb(II) and Cu(II) by an electrochemical sensor based on Zn/Ni-ZIF-8/XC-72/Nafion hybrid materials, *Environ. Res.* 202 (2021) 111605. <https://doi.org/10.1016/j.envres.2021.111605>.